J. Fluid Mech. (1972), *vol.* 54, *part* 4, *pp.* 691–717
Printed in Great Britain

Experiments on Taylor columns in rotating stratified fluids

By PETER A. DAVIES
School of Physics, University of Newcastle upon Tyne†

(Received 9 March 1972)

Experiments have been conducted to determine the effect of density stratification upon certain characteristic features of so-called Taylor columns. The interior structure of the homogeneous Taylor column is first of all described and compared with flow patterns obtained when the fluid is stratified. Qualitative features of the horizontal and vertical motion (in particular, the attenuation with height of the distortion created by the obstacle) are then described for values of the stratification parameter S (defined as $S = N/2\Omega$, where N and Ω are the Brunt–Väisälä and rotation frequencies respectively) in the range $0 \leqslant S \leqslant 0{\cdot}24$. The effect of density stratification upon, specifically, the length of the column is then described. A working definition for the existence of a Taylor column in a given experimental situation is formulated, enabling the strength of the column to be quantified at a particular height above the obstacle. Using this method the column length is measured as a function of S in the range $0 \leqslant S \leqslant 0{\cdot}24$. It is shown that even very slight stratification is sufficient to produce noticeable modification of all aspects of the flow. In particular, the column length is considerably reduced by weak stratification.

1. Introduction

The flow associated with the slow, steady, horizontal motion of a solid obstacle through a fluid rotating about a vertical axis has been considered. If the motion is steady and the fluid is homogeneous and inviscid, the Taylor–Proudman theorem (Proudman 1916; Taylor 1923) predicts that the imaginary upright cylinder circumscribing the obstacle can separate the flow into two regions. Outside this imaginary cylinder the fluid flows around it as if encountering a solid cylinder extending throughout the depth of the fluid, whilst inside the cylinder the fluid is at relative rest and moves with the obstacle. Such a cylinder is commonly referred to as a Taylor column after Taylor (1923), who first demonstrated the phenomenon. (In fact, strictly speaking, the Taylor–Proudman theorem does not predict that the fluid inside the column must necessarily be stagnant; any flow satisfying continuity with the streamlines following contours of constant depth is possible.)

Following the original experiments of Taylor, several attempts have been

† Present address, International Meteorological Institute, University of Stockholm, Sweden.

made to solve the problem theoretically (e.g. Stewartson 1953, 1967; Jacobs 1964*a*). Each of these theoretical attempts has been characterized by the particular ageostrophic term retained to remove the degeneracy inherent in the Taylor–Proudman theorem and by the particular geometrical configuration considered. [For a comprehensive bibliography see Hide, Ibbetson & Lighthill (1968).] Following a suggestion of Hide (1961) that the Great Red Spot on the planet Jupiter could be evidence of a Taylor-column-like phenomenon in the Jovian atmosphere, the original experiments of Taylor were repeated and extended (Ibbetson 1965; Hide & Ibbetson 1966; Hide *et al.* 1968). It was established (see also Vaziri & Boyer 1971) that in laboratory situations the fluid within the column was never stagnant, but had a rather complicated flow structure, even though ageostrophic effects were small. The dependence of certain features of this interior flow structure upon the relevant non-dimensional parameters of the problem was investigated. In view of the importance of both rotation and stratification in certain geophysical situations, much of the work on the Taylor column problem, including the present study, has been at least partly motivated by geophysical considerations. The steering of oceanic and atmospheric flows by bottom topography, for example, has been discussed specifically in terms of the Taylor-column phenomenon (by Stone & Baker 1968; Hide 1969, 1971) and more generally by Warren (1963, 1969), Robinson (1960), Hide (1963) and Jacobs (1964*b*).

In this paper we are concerned with the effects of varying degrees of density stratification upon the Taylor column (unless otherwise specified, 'Taylor column' will be taken to mean the imaginary upright cylinder circumscribing the obstacle). In the first part of the paper (§§ 4–6), following the introduction and definition of the basic parameters in § 2 and the description of the apparatus in § 3, the influence of the stratification on the horizontal and vertical flow patterns is described. For purposes of comparison the complete three-dimensional flow pattern for the *unstratified* case is first of all described and compared with the results obtained by previous workers. The stratified and non-stratified flow patterns are compared qualitatively and their attenuation with height, for a particular value of S, is described. In § 5.1 quantitative measurements of the decay with height of the vertical motion above the obstacle are presented and compared with results for the unstratified case.

In the second part of the paper measurements of the length of the Taylor column as a function of the stratification parameter S are presented. Because the fluid within the Taylor column is not stagnant for very small but finite Rossby and Ekman numbers, it is first of all necessary to formulate some criterion for the existence of a 'laboratory' Taylor column in a given experimental situation. This 'working definition', based upon the actual flows occurring in the column interior, then enables the length of the column to be quantified and the consequent modifications brought about by stratification to be gauged.

In § 8 of this paper, following the definition and discussion of the criterion adopted, experimental results are presented. Section 8.2 describes the decay with height of the Taylor column above a sphere, in terms of this criterion, for various S. From these results, estimates are made of the column length in each

case. The length of the unstratified column, under otherwise identical experimental conditions, is also measured. In § 8.4 the data are re-calculated to determine the velocities in the interior of the column for different S and for various heights above the obstacle, and the results are compared with direct experimental determinations of these velocities. Using both sets of calculations estimates of Taylor column length as a function of S are presented.

2. Basic equations and parameters of the problem

The equations of motion and continuity of a fluid of kinematic viscosity ν and density ρ, relative to a Cartesian co-ordinate system (x, y, z) rotating with angular velocity $(0, 0, \Omega)$, are

$$\frac{\partial \mathbf{V}}{\partial t} + \mathbf{V}.\nabla\mathbf{V} + 2\boldsymbol{\Omega} \times \mathbf{V} = -\frac{1}{\rho}\nabla p - \mathbf{g} + \nu\nabla^2\mathbf{V}, \tag{2.1}$$

$$\nabla.\mathbf{V} = 0, \tag{2.2}$$

$$\partial\rho/\partial t + \mathbf{V}.\nabla\rho = \kappa\nabla^2\rho, \tag{2.3}$$

where $\mathbf{V} = (u, v, w)$ is velocity, t is time, p is pressure, $\mathbf{g}$ is the acceleration due to gravity, and κ is a diffusivity coefficient. In (2.1) the centrifugal force is incorporated in $\mathbf{g}$; it is assumed that this does not make $\mathbf{g}$ significantly non-vertical.

Considering steady motions and splitting the density and pressure fields as follows:

$$\rho(x, y, z) = \rho_0 + \bar{\rho}(z) + \rho^*(x, y, z), \tag{2.4}$$

$$p(x, y, z) = p_0(z) + p^*(x, y, z), \tag{2.5}$$

(2.1), (2.2) and (2.3) become, within the Boussinesq approximation,

$$\mathbf{V}.\nabla\mathbf{V} + 2\boldsymbol{\Omega} \times \mathbf{V} = -\frac{1}{\rho_0}\nabla p^* - \frac{g\rho^*}{\rho_0}\mathbf{k} + \nu\nabla^2\mathbf{V}, \tag{2.6}$$

$$\nabla.\mathbf{V} = 0, \tag{2.7}$$

$$\mathbf{V}.\nabla\rho^* + w\,\partial\bar{\rho}/\partial z = \kappa\nabla^2\rho^*, \tag{2.8}$$

where $\mathbf{k}$ is a unit vector in the z direction. The quantity $p_0(z)$ in (2.5) is defined by

$$\partial p_0(z)/\partial z = -g(\rho_0 + \bar{\rho}(z)).$$

With the introduction of the scaling

$$\mathbf{V} = U\mathbf{V}', \quad \nabla = (1/L)\nabla', \quad p^* = 2\Omega U\rho_0 L p^{*\prime}, \quad \rho^* = 2\Omega U\rho_0 g^{-1}\rho^{*\prime}, \quad \bar{\rho} = R\bar{\rho}',$$

(2.6)–(2.8) become (dropping primes)

$$\epsilon\mathbf{V}.\nabla\mathbf{V} + \mathbf{k} \times \mathbf{V} = -\nabla p^* - \rho^* + E\nabla^2\mathbf{V}, \tag{2.9}$$

$$\nabla.\mathbf{V} = 0, \tag{2.10}$$

$$\epsilon\mathbf{V}.\nabla\rho^* + S^2 w\,\partial\bar{\rho}/\partial z = \sigma^{-1}E\nabla^2\rho^*, \tag{2.11}$$

where $\epsilon = U/2\Omega L$, $E = \nu/2\Omega L^2$, $\sigma = \nu/\kappa$ and $S = N/2\Omega$, with N, the Brunt–Väisälä frequency, given by $N^2 = gR/\rho_0 L$. In the experiments to be described $\sigma \gg 1$ and the effects of rotation and stratification dominate inertial and viscous effects. That is

$$\epsilon \ll 1, \quad E \ll 1, \quad S \lesssim 1,$$

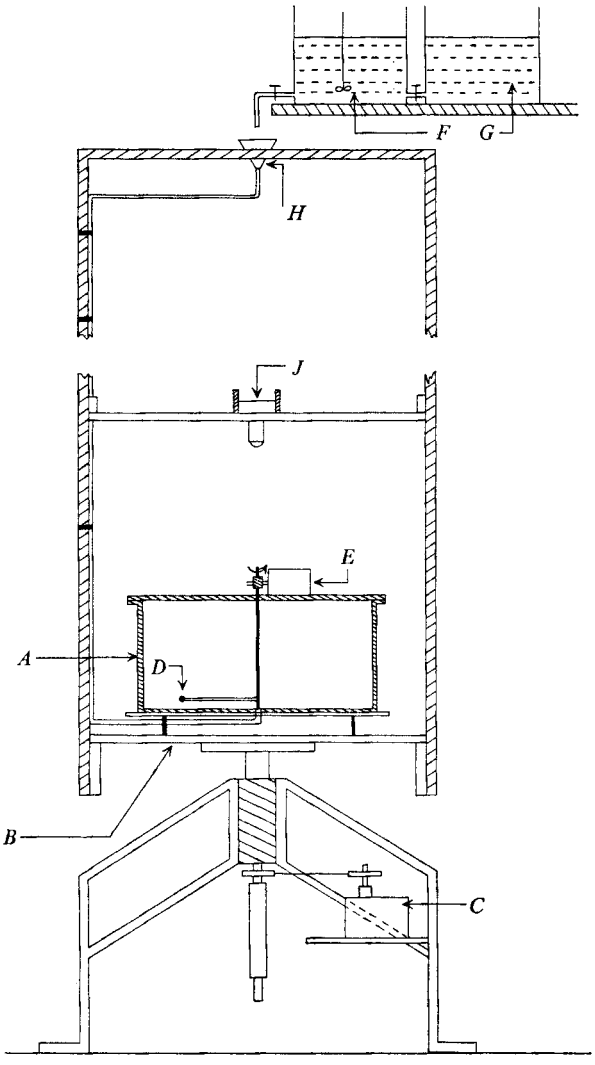

FIGURE 1. Schematic diagram of the experimental apparatus.

where E, ϵ and S, as defined above, are the Ekman number, Rossby number and stratification parameter respectively.

In the special limiting case of $E \to 0$ and $\epsilon \to 0$ equation (2.9) reduces to the equation of geostrophy, and under the further constraint of $S = 0$, fluid motions obey the Taylor–Proudman theorem precisely.

3. The apparatus

A schematic diagram of the experimental apparatus is shown in figure 1. The main features of the arrangement were the following.

(*a*) A Perspex tank A which could be filled with working fluid and rotated on a turntable B driven by an electric motor C.

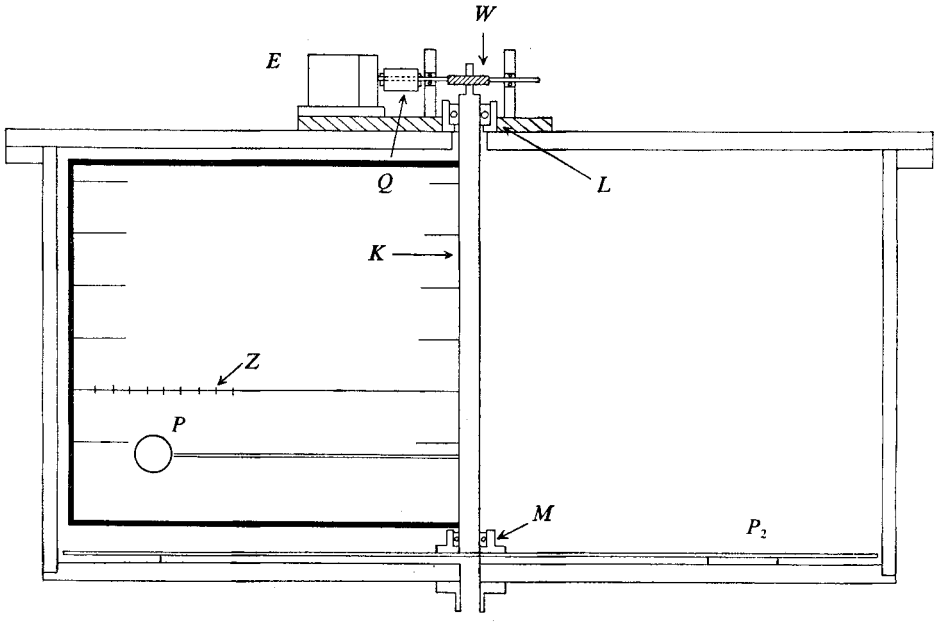

FIGURE 2. Details of the tank assembly.

(*b*) An obstacle *D* which could be differentially rotated through the fluid by means of a small d.c. motor *E* attached to the top surface of the tank.

(*c*) An arrangement for filling the tank *A* with fluid whilst the apparatus was rotating. Reservoir tanks *F* and *G* and the funnel *H* were the principal components of this assembly.

(*d*) A photographic arrangement *J* supported on vertical struts attached to the table at its edges. [Details of the construction of the rotating table *B* and the accompanying slip-ring assembly have been described elsewhere (Davies 1971).]

The tank, which had a fixed base and removable top lid, was made from 1 cm thick Perspex and had a diameter of 61 cm and height of 30·5 cm. By being slightly raised above the table by three screw supports, it could be filled through a hole in its base whilst rotating. A white Perspex base plate, of slightly smaller diameter than the tank, was placed on 4 mm spacers bolted to the top surface of the tank base; the small gap between the tank wall and the edge of this base plate then allowed the main body of the working volume to be filled slowly without any disturbance from the inlet fluid. The arrangement for moving an obstacle slowly through the fluid can be seen on figure 2. In this case the obstacle was a sphere *P* made of Perspex, which was attached to a central shaft *K* by a light radial arm. The centre of the sphere rotated in a horizontal plane, describing a circular path of radius $r = R$. The central shaft was driven by the miniature d.c. motor *E* through a flexible coupling *Q* and worm gear arrangement *W* and ran on two sealed bearings *L* and *M*.

Horizontal flow patterns were recorded using a Nikon F 35 mm camera (*J*) mounted on the table, and photographs were also taken looking radially into

the tank using a second camera stationary in the laboratory. Light for the photography was provided by an array of 8 fluorescent lights attached to the rotating table.

The tank was filled, whilst rotating, by the method of stratification described typically by Oster (1965). Concentrated salt solution (in these experiments calcium chloride was the salt used) and water were stored in reservoirs G and F respectively and, by suitably adjusting the reservoir taps and continuously agitating F, a linear density gradient could be produced in the tank A. The tank was filled slowly (typically over 12 hours) to avoid excessive mixing and left to spin up to solid-body rotation.

3.1. *Flow visualization*

The method of flow visualization used throughout was the well-established pH-indicator technique (Baker 1966). A vertical array of horizontal dye-release wires Z (see figure 2) was supported on a rectangular, rigid frame and attached to the obstacle drive shaft K. The array was off-set typically two sphere diameters in front of the obstacle, enabling dye to be released from the wires ahead of the sphere as it rotated. The wires, which were tautly attached to the rectangular frame, were situated at irregular but specified heights above the sphere and were insulated from each other because of the special construction of shaft K. In this way, by means of a switch and slip-ring assembly it was possible to scan vertically through the fluid and look at the flow at different heights independently. The wires used for the release of dye were 0·025 cm diameter copper wires and a d.c. potential could be impressed between them and a large brass ring electrode secured to the lower surface of the tank lid. In order to improve the dye 'thickness' when viewed from above, the dye-release wires had a rake-like form with small vertical prongs of the same gauge wire soldered along their length (see figure 2). Difficulties were encountered with bubbling at the electrodes because dissolved salt was used to stratify the fluid, and this limited the intensity of the dye produced. This necessitated rather careful titration of the solutions before mixing, and the use of low voltages.

4. Experiments with $S = 0$

In order that meaningful comparison could be made between flow patterns observed in the cases $S = 0$ and $S \neq 0$, it was necessary, first of all, to determine the complete 3 dimensional flow field produced by the spherical obstacle, with the fluid unstratified. Some of the separate features of this 'homogeneous' flow field have been investigated by earlier workers; for example the *vertical motion* in the Taylor column above a solid sphere was studied by Hide *et al.* (1968). By repeating some of these experiments and by qualitatively repeating with a spherical obstacle the earlier experiments of Hide & Ibbetson (1966) (who studied the flow over a right circular cylinder and over radial arms of various cross-section) the complete reference flow pattern could be determined.

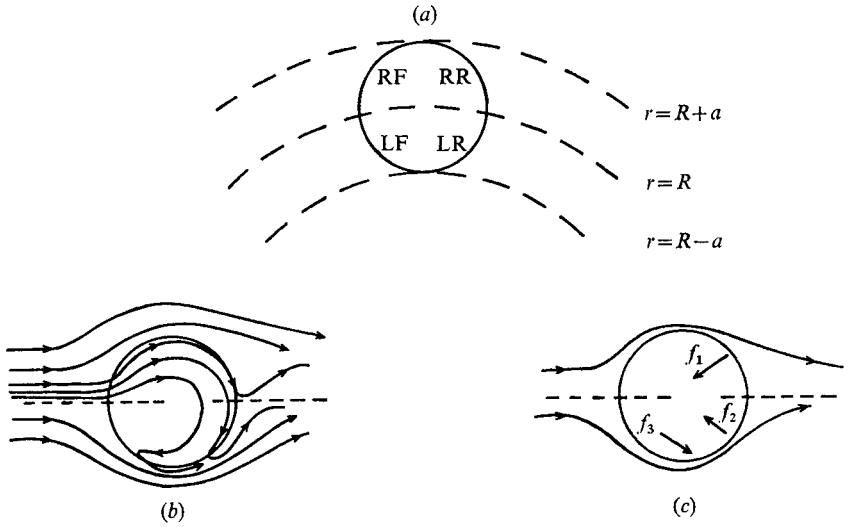

FIGURE 4. Schematic representation of the horizontal flow pattern for $S = 0$. (*a*) Definition (RF = right front, LR = left rear etc.) of the system of reference used. The flow within the column interior is shown (*b*) schematically and (*c*) in terms of f_1, f_2 and f_3.

4.1. *Description of interior flow structure for* $S = 0$

The values of the non-dimensional parameters ϵ and E in the $S = 0$ experiments were used throughout the unstratified and stratified experiments, that is

$$\epsilon = 8{\cdot}8 \times 10^{-3}, \quad E = 4{\cdot}0 \times 10^{-4}.$$

The length scale on which the above parameters are based is a, the radius of the sphere ($a = 1{\cdot}9$ cm). Figure 3 (*a*) (plate 1) shows a flow pattern obtained in the unstratified case looking down on the obstacle. In this figure the dye has been released at a height of one obstacle radius above the top of the sphere. When the fluid is homogeneous such horizontal flow patterns display the same gross features at all heights above the obstacle. However, changes in detail with height in both the horizontal and vertical flow fields are observed, as is described later in this section.

Flow patterns such as that in figure 3 (*a*) showed strong similarities with those obtained by Ibbetson (1965) with cylindrical obstacles, especially in regard to the basic asymmetry of the flow and the rather complicated nature of the secondary flows within the column. Once the dye lines have penetrated the interior of the column they can be seen to be deflected horizontally as shown schematically in figure 4 (*b*). There is some vertical motion within the column also, such that the dye lines try to follow the contours of the sphere. This aspect of the flow has been extensively investigated by Hide *et al.* (1968).

The region of three-dimensional distortion inside the column is quite well-defined, as can be seen from figure 3 (*a*). Relative to a frame of reference fixed in the obstacle, the magnitudes of the flows within the column are slow compared with the basic stream velocity and have directions very similar to those observed by Ibbetson (1965). The time development of the dye pattern has been observed

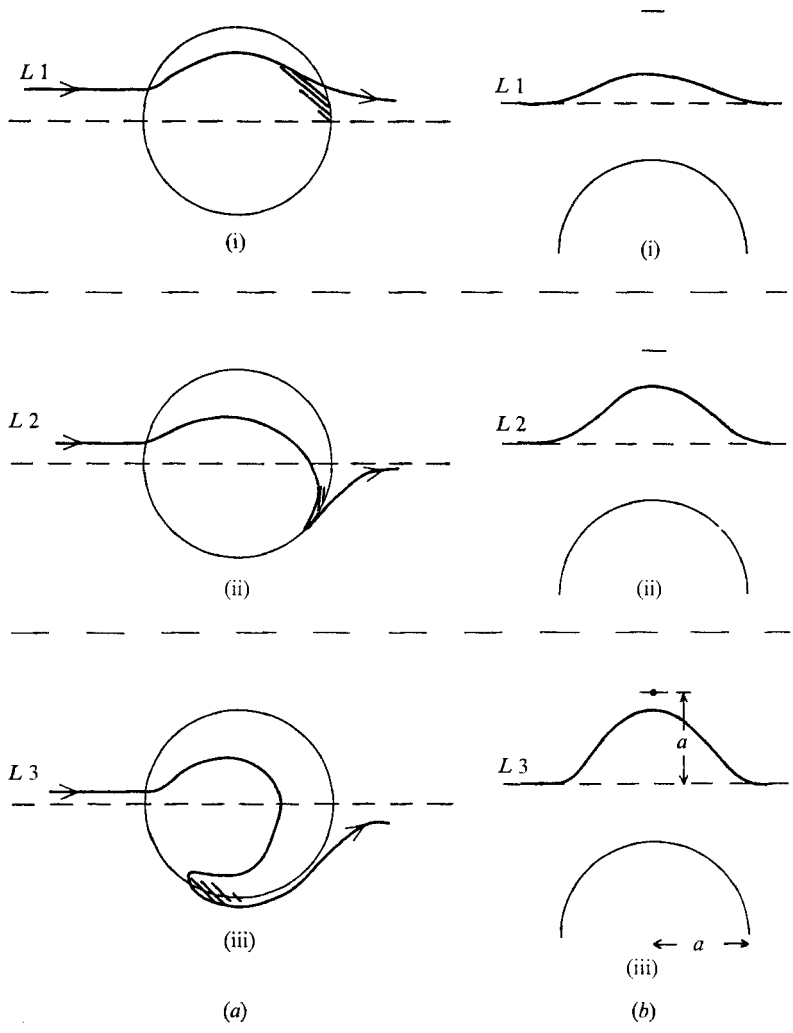

FIGURE 5. Diagram illustrating (*a*) horizontal and (*b*) vertical distortions experienced by dye lines (i) $L1$, (ii) $L2$ and (iii) $L3$ for some given height above the obstacle (whose radius is a).

in order to obtain an estimate of the magnitudes of such 'secondary' flows. Because the degree of vertical distortion of a particular dye line in the interior of the column is determined by its initial radial displacement from the circle of radius $r = R$ (see figure 4(*a*)) the time development of each dye line is different until the overall dye pattern becomes steady. This development in time, for some chosen height above the obstacle, can be classified into three stages by considering typical dye lines such as the lines 1, 2 and 3 ($L1$, $L2$ and $L3$) shown in figure 5. The vertical distortion experienced by each of these lines, at this chosen height, is also illustrated on this figure (figure 5(*b*)).

Dye lines which have penetrated the column near its right-hand boundary, such as $L1$, undergo relatively small vertical movement and are only slightly horizontally deflected as shown. For dye lines originating nearer the centre-line,

$r = R$, there is larger vertical distortion in the column as a result of the surfaces of constant height being hemispheres. The maximum vertical distortion thus occurs in the neighbourhood of point B in figure 3 (a).

A dye line such as $L2$ (see figures 5 (a, ii) and (b, ii)) is deflected horizontally much more sharply and its speed across the interior is correspondingly slower than that of $L1$ nearer the edge of the column. At the rear of the column there is some attachment to the column walls and, consequently, a rather ill-defined slow drift of fluid takes place through these walls. This feature of the flow, observed for all lines, is illustrated by shading on figure 5.

Dye line 3 (see figures 5 (a, iii) and (b, iii)), which takes the longest time to traverse the column and which undergoes maximum vertical distortion, i.e. the dye line passing through point B on figure 3 (a), is seen to be deflected almost back on itself at the rear left of the column. Under the influence of flow f_3 (see figure 4 (c)) it then moves back to the rear left and leaves the interior as shown on figure 5 (a, iii).

The composite steady dye pattern, which can be said to be present when the critical dye line 3, passing through point B (see figure 3 (a)), has traversed the column and escaped from the interior, was found to be set up in a time which implied a mean secondary flow across the interior of the order of $\frac{1}{10}U$ (U being the obstacle speed). The magnitude of this interior flow, and its dependence upon the relevant non-dimensional parameters of the problem, has subsequently been investigated more fully.

Thus far, consideration has been given to dye lines originating at the right-hand side of the column, i.e. at radii $r > R$. Dye lines which approach the left front of the column, i.e. those satisfying $(R-a) < r < R$, did not appear to penetrate the column though, at the edge of the column, some downward vertical distortion could be seen. Although this aspect of the flow was not systematically investigated it seemed that, for a particular height above the obstacle, the magnitude of the downward distortion was less than, but of the same order as, η, the upward distortion in the column interior.

4.2. *Variation of interior flow structure with height for* $S = 0$

Some qualitative observations were made to determine any variations in the flow pattern with the vertical co-ordinate z. The gross features of the steering of the flow by the obstacle remained unaltered, except that the wake region extended further round towards the left rear of the column with increasing z (see figure 3 (b)). Measurements on the attenuation with height of the interior vertical distortion η showed good agreement with the results of Hide *et al.* (1968) in (a) the form of the attenuation and (b) its $E^{\frac{1}{4}}$ dependence.

Modifications to the horizontal structure of the interior flow were also observed as z increased. Whilst the pattern of penetration within the column still appeared to be quite well defined, dye previously released ahead of the column filled more of the interior than had been the case just above the sphere. This difference can be seen by comparing figures 3 (a) and (b); figure 3 (b) shows the flow pattern at a height above the obstacle of approximately 7 obstacle radii. The flow directed

towards the interior from the left rear of the column, whilst still slow, is relatively much stronger in figure 3(*a*) than in figure 3(*b*). This results in the dye in figure 3(*b*) being able to drift further into the column, moving very slowly and spreading out considerably before being influenced by the reverse flow, denoted by f_3', which takes it out into the main stream. This reverse flow f_3' appears to originate much nearer the front of the column than does the analogous f_3 in figure 4(*c*), such that an inner dye line turns almost to meet itself before being taken out of the interior. Figure 3(*b*) shows a small, seemingly unpenetrated region within the column, and it seems probable that this is a region of closed streamlines analogous to such regions observed by Hide & Ibbetson (1966) in their experiments.

5. Experiments with $S \neq 0$

After the three-dimensional flow field associated with the slow steady motion of a spherical obstacle through a rotating *homogeneous* fluid had been determined, the experiments were repeated with the fluid density-stratified. The degree of modification to the typical $S = 0$ flow pattern was, of course, dependent upon the values of S and z/a (the normalized distance above the top of the sphere, radius a) in the particular experiment, as can be seen from figures 6–9. These figures each show, in sequence, the flow patterns obtained by releasing dye ahead of the obstacle at different heights in the fluid for values of S of 0·12, 0·13, 0·16 and 0·26 respectively. All the sets of figures have been traced from photographs for clarity and the distances marked are vertical distances above the top of the sphere. Shading is used to represent the spreading of the dye and dotted lines are employed when the intensity of the dye was such that the path of the dye line was not completely distinct.

Comparison of figures 6–9 with the corresponding figures for $S = 0$ (i.e. figures 3(*a*) and 3(*b*)) illustrates the important similar features in the horizontal flow patterns. Near the obstacle, when the fluid is stratified, for example, as in figure 6, there is deflexion of the outer dye lines just as is found with the classical Taylor column. With this column defined as before as the upright cylinder circumscribing the obstacle, there is flow through the column 'walls' for all heights and a deceleration of the flow within the column. Observations (Davies 1971) have shown that the magnitude of this deceleration was strongest near the obstacle and became weaker with increasing height, for all S. Just as with the $S = 0$ case the form of the flow within the column was three-dimensional with observable vertical motions accompanying any horizontal distortion of dye lines. Inside the column interior the pronounced deflexion and spreading out of dye lines, a characteristic of the $S = 0$ flow patterns, was seen to vary considerably with z and, in particular, the secondary flow observed in $S = 0$ experiments directed from the left rear of the column towards the interior appeared much weaker or indeed absent when the fluid was stratified.

The closest similarities in $S = 0$ and $S \neq 0$ flow patterns were seen for lowest values of z, i.e. at heights just above the obstacle, such as $z = 0{\cdot}1$ cm on figure 6. For such positions the dominant secondary flow appeared to be analogous to the

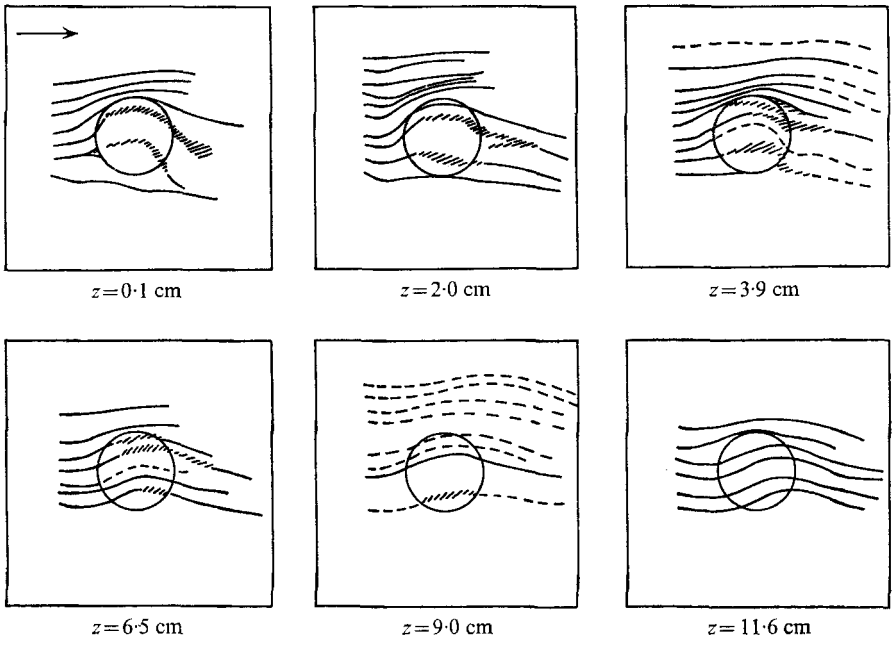

FIGURE 6. Horizontal flow patterns for $S = 0{\cdot}12$ at various heights above the obstacle. Direction of flow is from left to right as indicated. Sphere radius a is 1·9 cm.

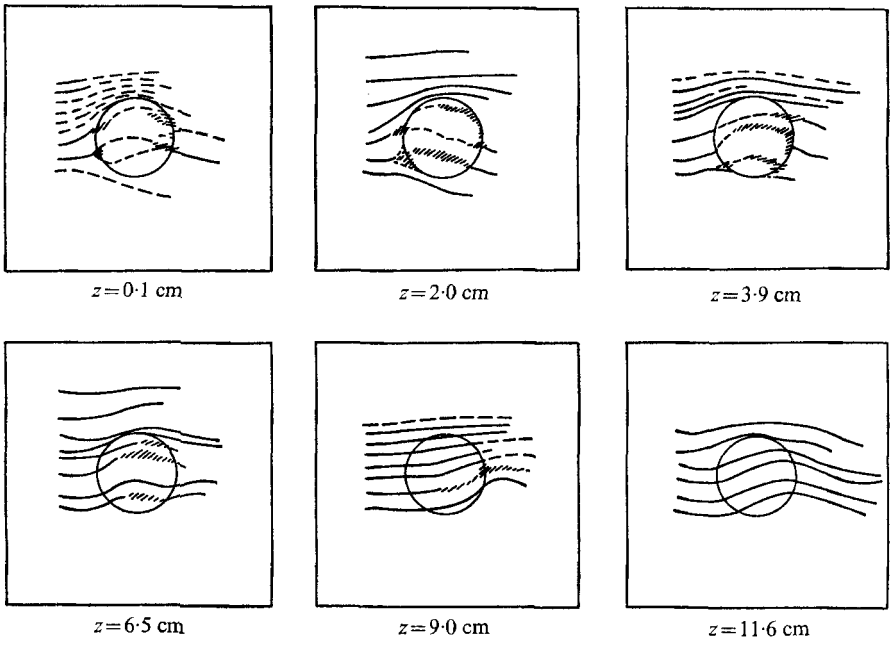

FIGURE 7. Horizontal flow patterns for $S = 0{\cdot}13$. Other conditions as in figure 6.

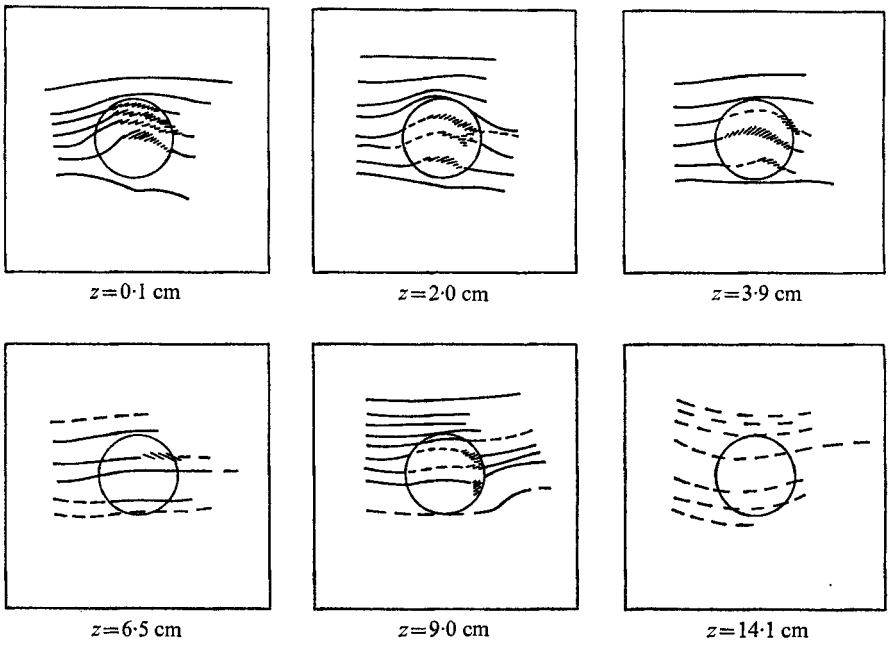

FIGURE 8. Horizontal flow patterns for $S = 0{\cdot}16$. Other conditions as in figure 6.

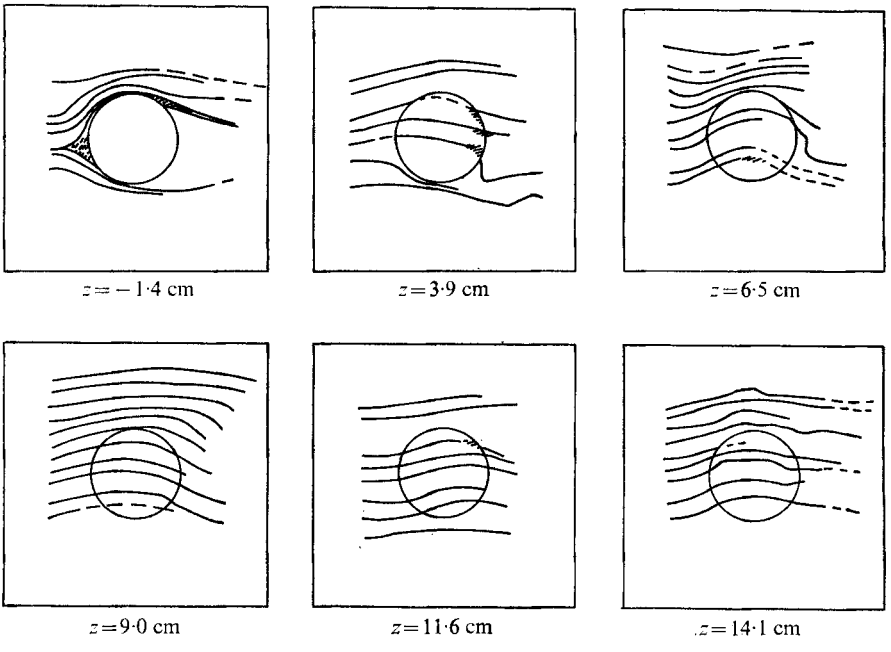

FIGURE 9. Horizontal flow patterns for $S = 0{\cdot}26$. Other conditions as in figure 6.

flow f_1 for $S = 0$. As the value of z increased, the deflexions became less pronounced until the flow state approached a uniform streaming across the column, with very little distortion or deceleration of dye lines taking place. The value of z at which this flow was observed was dependent upon the value of S, as can be seen from figures 6–9.

Figures 6–9 also show that, where there was marked steering of the flow by the obstacle, the associated secondary flow within the column was, in some sense, simpler than in the unstratified case. In particular there appeared to be no strong reverse flows analogous to f_2 and f_3 in the interior, even very near the obstacle or for low values of S (say $S < 0{\cdot}1$). The slow transport of fluid out through the rear wall of the column is strongly similar to the $S = 0$ behaviour. This feature became less pronounced as the deflexion of penetrating dye lines decreased (see figures 6 and 9).

5.1. *Vertical motion in the column interior for* $S \neq 0$

As in the unstratified case, motions in the interior of the column were three-dimensional with dye lines trying to follow the hemispherical shape of the obstacle whilst undergoing horizontal distortion. Photographs of this vertical motion for several values of S can be seen on figure 10 (plate 2). It was found that for values of S greater than about $S = 0{\cdot}15$ the amplitude of the vertical motion in the column interior was susbstantially less than the amplitude of such motion for $S = 0$, at the same reference height above the obstacle. At heights of one sphere radius or more above the obstacle, vertical distortions were very small and difficult to measure accurately for the highest values of S. However, for values of S less than $S = 0{\cdot}1$, the attenuation with height of the normalized vertical displacement, η/a, was measured for three values of S. Figure 11 shows the form of this attenuation for values of S of 0·07, 0·08 and 0·09 respectively. The $S = 0$ case is shown for comparison. Reference to figure 11 shows that, whilst its magnitude has been reduced, the *form* of the decay of η/a with height is essentially the same as when the fluid is unstratified. In addition, it was observed that several features of the vertical motion within the column were common to both stratified and unstratified cases: in particular, the downward distortion at the left-hand side of the column accompanying the main upward distortion in the column interior.

The effects on the vertical flow brought about by changing S can be illustrated by comparing η/a with S for a particular height above the obstacle, $z = Z_h$. To incorporate the maximum amount of experimental data it was necessary that this value, Z_h, should be small, i.e. the comparison should be made near the obstacle. Such a comparison is shown on figure 12, which is a plot of η/a against S at a height of 0·1 cm above the top of the sphere. Because all points on this graph are subject to large error, the curve should be regarded only as an indication of the trend of the results. In spite of the large errors this graph shows that, even extremely close to the obstacle, the effect of stratification is felt. As in figure 11, even for very small values of S the vertical distortion in the column is reduced by an amount of the order of 20 % from its value in the $S = 0$ case, i.e. for values of S where most data has been collected (between $S = 0{\cdot}05$ and $0{\cdot}1$).

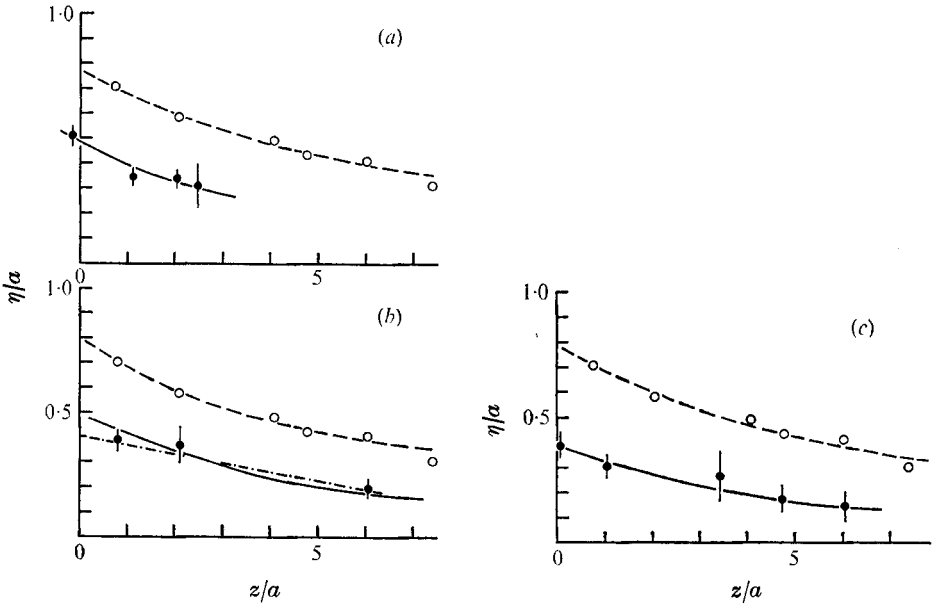

FIGURE 11. Plots of η/a against z/a for several values of S. – –, $S = 0$ for comparison. (*a*) ——, $S = 0{\cdot}07$; (*b*) ——, $S = 0{\cdot}08$; –·– $S = 0{\cdot}08$ linear fit. (*c*) ——, $S = 0{\cdot}09$.

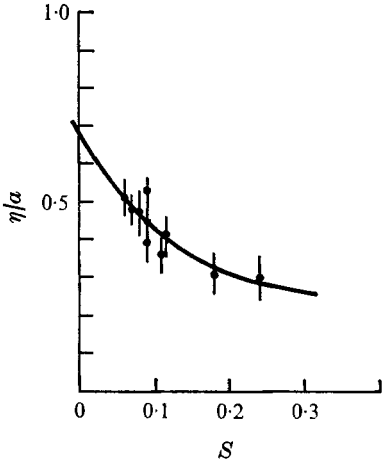

FIGURE 12. Plot of η/a against S for $Z_h = 0{\cdot}1$ cm.

Towards the top of the range of S, the graph on figure 12 shows signs of levelling off, compared with $S < 0{\cdot}1$ behaviour, and for $S = 0{\cdot}24$ the maximum distortion at $z = Z_h$ is of the order of 0·4 times its value for $S = 0$ at this height.

6. Summary

Before proceeding to describe the more quantitative part of the investigation, it is of interest here to summarize the results obtained so far. It is convenient, for purposes of comparison, to consider separately the horizontal and vertical

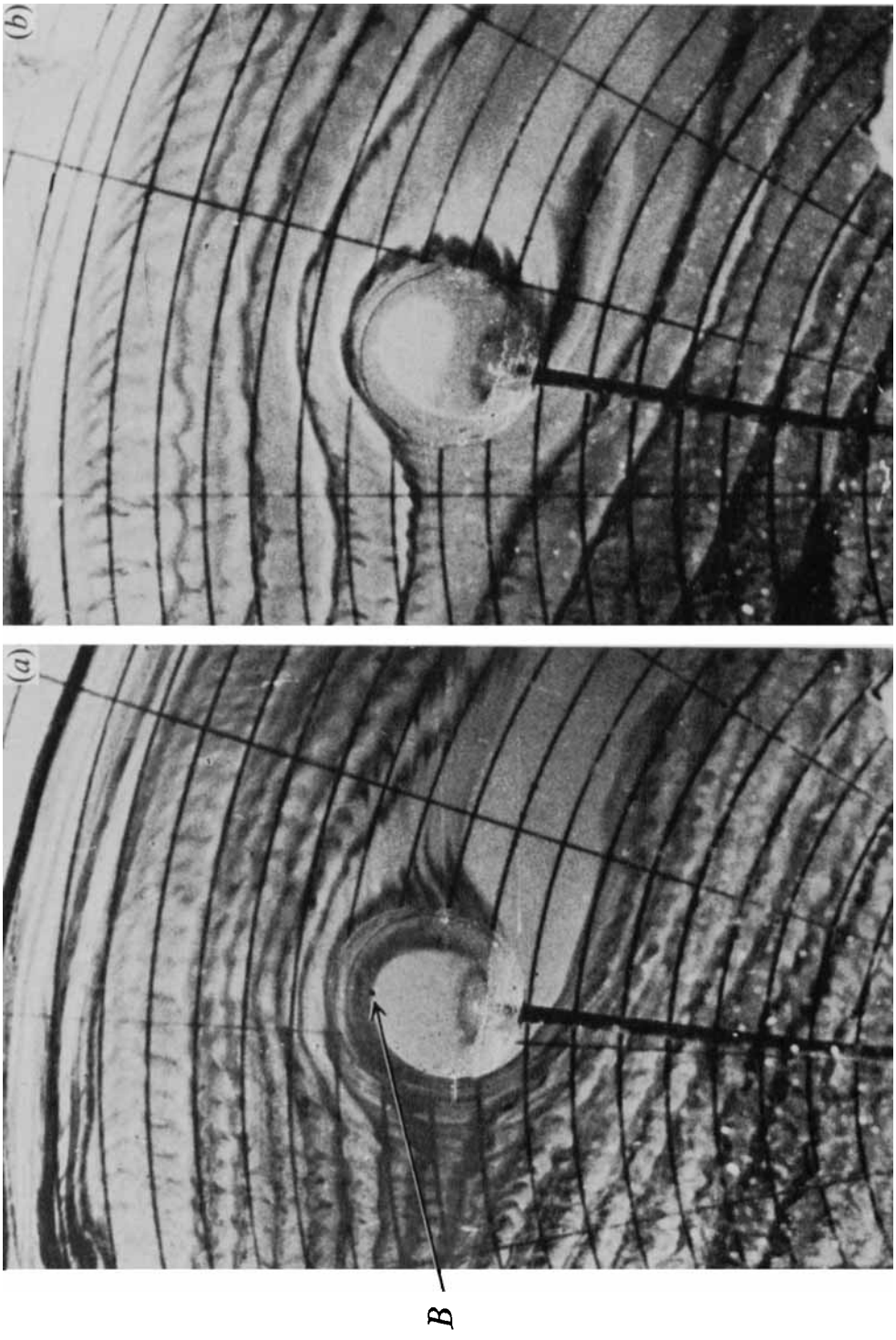

FIGURE 3. Plan views of the flow over a spherical obstacle with the fluid unstratified. The direction of the stream is from left to right and dye is being released at (*a*) one sphere radius and (*b*) seven sphere radii above the top of the obstacle. The sense of Ω is anticlockwise and point B is a reference point (see text).

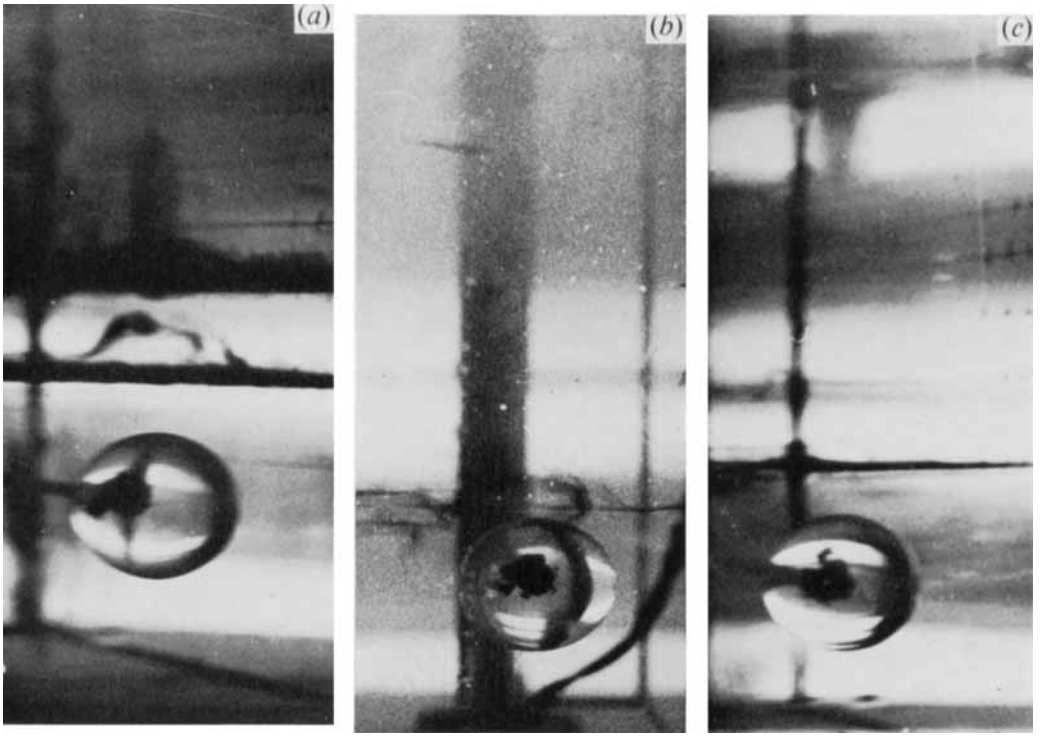

FIGURE 10. Vertical motion within the column for (*a*) $S = 0$, (*b*) $S = 0{\cdot}07$ and (*c*) $S = 0{\cdot}08$. The direction of flow is from right to left.

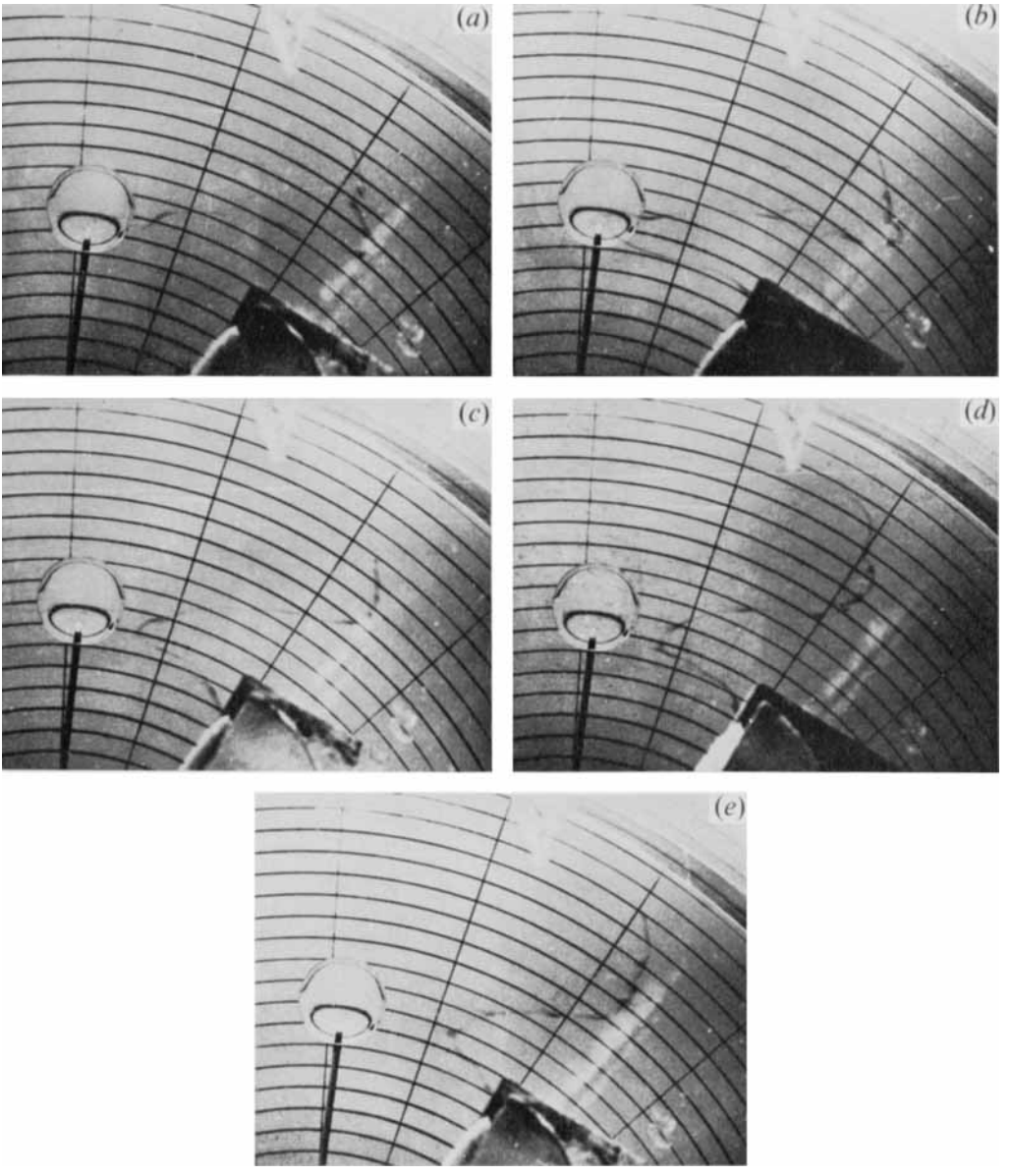

FIGURE 15. Dye line profiles for $S = 0{\cdot}24$ for (*a*) $z/a = 0{\cdot}8$, (*b*) $z/a = 4{\cdot}1$, (*c*) $z/a = 4{\cdot}8$, (*d*) $z/a = 6{\cdot}0$, (*e*) $z/a = 7{\cdot}4$.

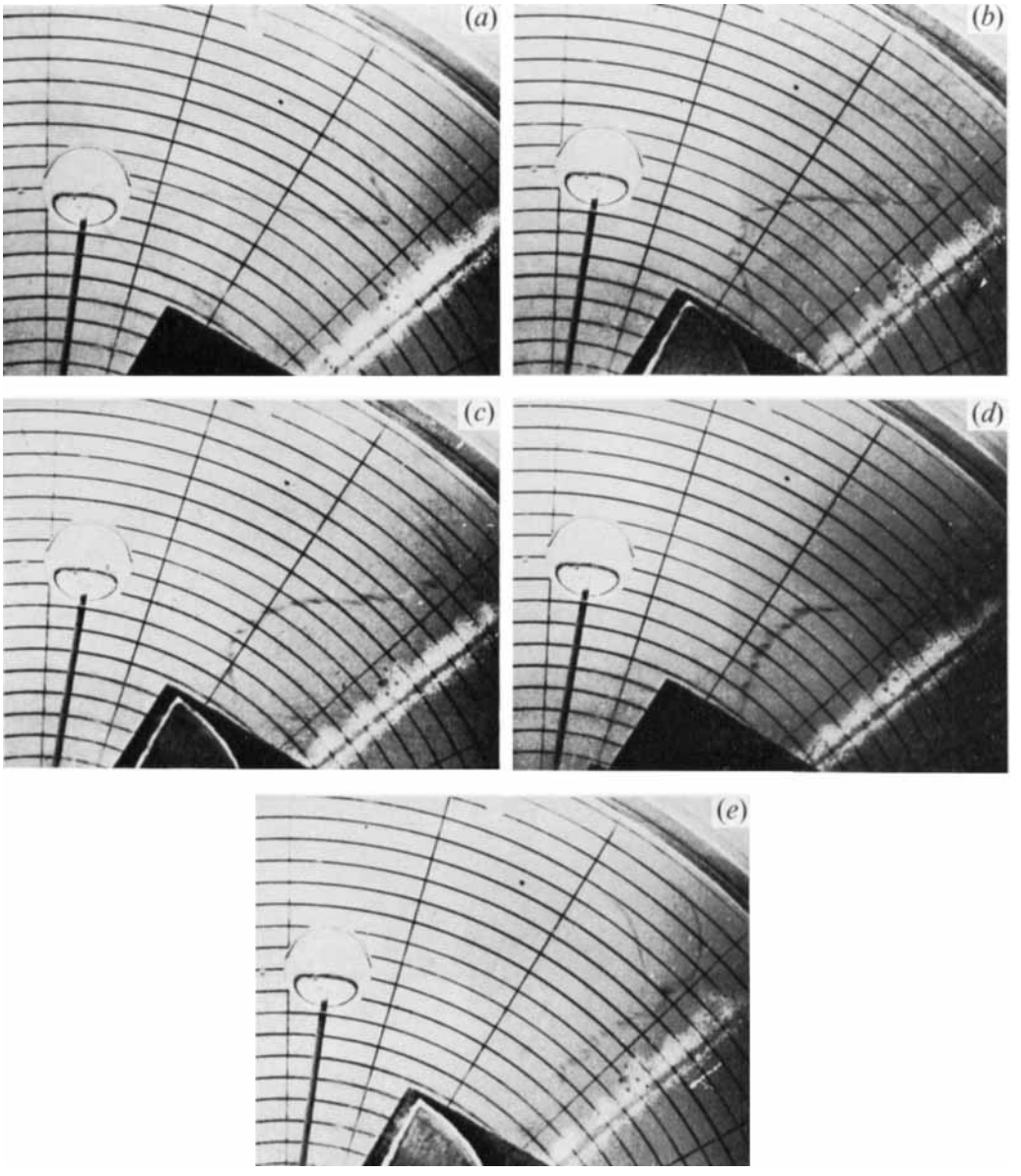

FIGURE 16. Dye line profiles for $S = 0{\cdot}115$ for (*a*) $z/a = 0{\cdot}8$, (*b*) $z/a = 2{\cdot}1$, (*c*) $z/a = 4{\cdot}1$, (*d*) $z/a = 4{\cdot}8$, (*e*) $z/a = 6{\cdot}0$.

flow patterns in the interior of the Taylor column. Particularly with the horizontal flow patterns the limitations brought about by difficulties with the flow visualization were quite serious. Detailed information concerning the interior flows within the column was not obtained as with the $S = 0$ case, and only qualitative conclusions can be drawn.

It was seen that very near the obstacle and for weak stratifications (i.e. $S < 0{\cdot}1$) the horizontal flow within the column was very similar to the typical $S = 0$ pattern. A strong reverse flow analogous to flow f_2 in the homogeneous case was not observed in this range and it appeared that this flow was either absent or very weak. Consequently, pronounced deflexion of dye lines occurred when $S < 0{\cdot}1$, especially near the obstacle, but dye lines spent much less time in the column than in the corresponding $S = 0$ situation. This is illustrated by the exit positions of typical dye lines in the two cases: when $S \neq 0$ this position is at the rear of the column close to the projection of the undisturbed path line and not near the left front of the column as with the $S = 0$ case.

The graphs in figures 11 and 12 (direct plot of the variation of η with S), in spite of the large errors on the points, do give a rather more quantitative indication of the effects of stratification. The graphs shown on figure 11 suggest that the forms of the decay relationships for $S = 0{\cdot}07$, $0{\cdot}08$ and $0{\cdot}09$ are very similar and, more significantly, they all show close resemblance to the corresponding decay curve for $S = 0$. The decrease in magnitude of η with S, for a given value of z, is easily seen. On figure 11, graph (a), for example, there is a reduction η of the order of 40 % for all measured z, even with slight stratification, a value of $S = 0{\cdot}07$ corresponding to a density gradient of 2×10^{-4} (g/cc) cm^{-1}. It is concluded that this reduction, as S takes small but non-zero values, is due to the presence of the density gradient. Clearly the use of dissolved salt to produce the density gradients resulted in an increase in the viscosity of the fluid. However, measurements of this increase with salt concentration showed that, in the range of S covered by figure 11, this effect was negligible. The negligible effects of viscosity as a contributory cause of the observed reduction in η is also consistent with the results of Hide *et al.* (1968), who found that an increase in viscosity of the fluid gave rise to a shortening in length of the Taylor column, but that the value of η *near* the obstacle was "more or less independent of E". Since graphs (a), (b) and (c) on figure 11 all show appreciable reductions in η for all z it is thought that this is caused by the presence of the density gradient and is not due, for example, to any increase in the viscosity of the fluid.

7. The length of the Taylor column

7.1. *Experimental observables*

The method adopted as a means of quantifying the strength of a 'laboratory' Taylor column can be illustrated by reference to figure 13. At some time, say $t = t_0$, as the obstacle moves along its path a line of dye is produced at a height $z = z^*$ above it and approximately two sphere diameters ahead of it. For a given S, the degree of distortion of the dye line is indicative of the strength of the column at that value of z. For example, in the case of the 'classical' Taylor column in

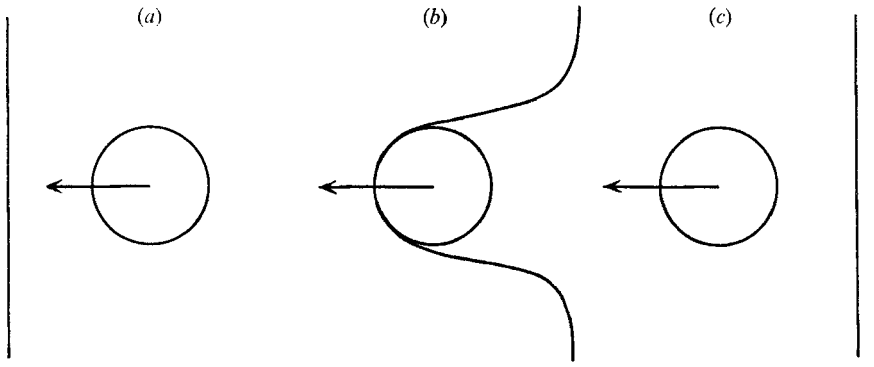

FIGURE 13. Distortion of a line of dye at times (a) $t = t_0$, (b) $t = t_1$ (classical Taylor column) and (c) $t = t_1$ (no column). The motion of the obstacle is from right to left, as shown.

a homogeneous fluid, where there is no flow through the column walls, at some later time $t = t_1$ the form of the dye line will be similar to that in figure 13(*b*). In this case the distortion is independent of z. In the other extreme case, if the Taylor column is completely absent at $z = z^*$, the presence of the sphere will not be detected and the dye line will remain undisturbed as in figure 13(*c*). Between the extremes illustrated by figures 13(*b*) and (*c*) there exist distortions which depend not only upon z but also upon S. The strength of the column can thus be quantified by the degree of distortion caused to an undisturbed dye line for a fixed $(t_1 - t_0)$.

Previous workers have also formulated 'working definitions' for the existence of a Taylor column in a given laboratory situation. For example, Ibbetson (1965) used a criterion based upon the magnitudes of the secondary horizontal flows (see § 4.1) in the column interior; in his experiments a Taylor column was said to be present if the velocities f_1 and f_2 were less than some arbitrary value.

Hide *et al.* (1968) used the vertical motion in the column interior to measure the Taylor column length. By measuring the attenuation of η with z it was found that the variation of η could be well-represented by the relationship

$$(\eta/a)_{z=z_m} = (\eta/a)_{z=0}\,(1 - z_m/z_c),\dagger$$

where $(\eta/a)_{z=z_m}$ is the normalized vertical distortion at the level $z = z_m$. z_c was the length of the Taylor column, defined as the value of z/a for which there was no vertical distortion.

The observable adopted in the present experiments and outlined earlier was found to be very sensitive. In particular, the method could indicate the influence of the spherical obstacle by the distorted dye line, when vertical distortion could not be detected. Furthermore, because of the experimental set-up the method was judged more applicable than on based upon the values of f_1 and f_2 in the present experiments.

† Different notation from that of Hide, Ibbetson & Lighthill (1968).

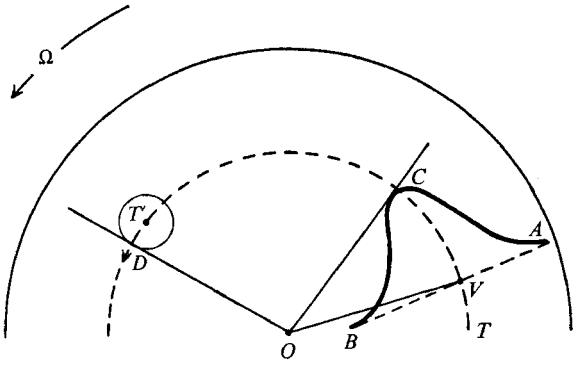

FIGURE 14. Schematic plan view of apparatus illustrating dye-line distortion created by the passage of the spherical obstacle.

7.2. *Notation*

Figure 14 shows part of a plan view of the apparatus. The spherical obstacle is differentially rotated through the fluid on a circular path, centre O, in the sense shown. The basic rotation Ω is in the direction indicated. At some time $t = t_0$ when the centre of the sphere is at point T, a straight line of dye AB is produced. At some time later, $t = t_1$, when the centre of the sphere has reached point T', the dye line is distorted into a typical profile ACB. The angle subtended at O by the arc VC, i.e. the angle through which the line AB has been distorted in a time $t_1 - t_0$, is denoted by the angle θ. The angle subtended at O by the arc VD, i.e. the angle through which the line AB would have been distorted by a 'classical' Taylor column, is denoted by θ_0.

Using this notation, the 'strength of the Taylor column' is defined by the ratio θ/θ_0 and can thus take values between zero and unity. (Since θ/θ_0 is slightly dependent upon θ_0 a reference value for θ_0 is necessary for internal consistency; the reference value chosen was $\theta_0 = 30°$.)

8. Experimental results

The apparatus used in these experiments has been described in § 3. The line of dye, necessary for measurements of θ/θ_0, was produced by the application of a voltage pulse on a thin horizontal wire, using the pH technique outlined earlier. It was ensured that the nature of the pulses was as standard as possible so that any distortion observed could be attributed to the effect of the obstacle and not to any differing polarization disturbances at different wires. With the pulsing unit used it was possible to vary both the amplitude and duration of the pulse. In this way it was possible to minimize polarization difficulties whilst still retaining sufficient dye contrast for photographic measurements to be made.

It was ensured that the parameters ϵ and E did not vary between each experimental run. The same sphere was used throughout the experiments and both the main rotation rate Ω and the differential rotation rate ω had the same given

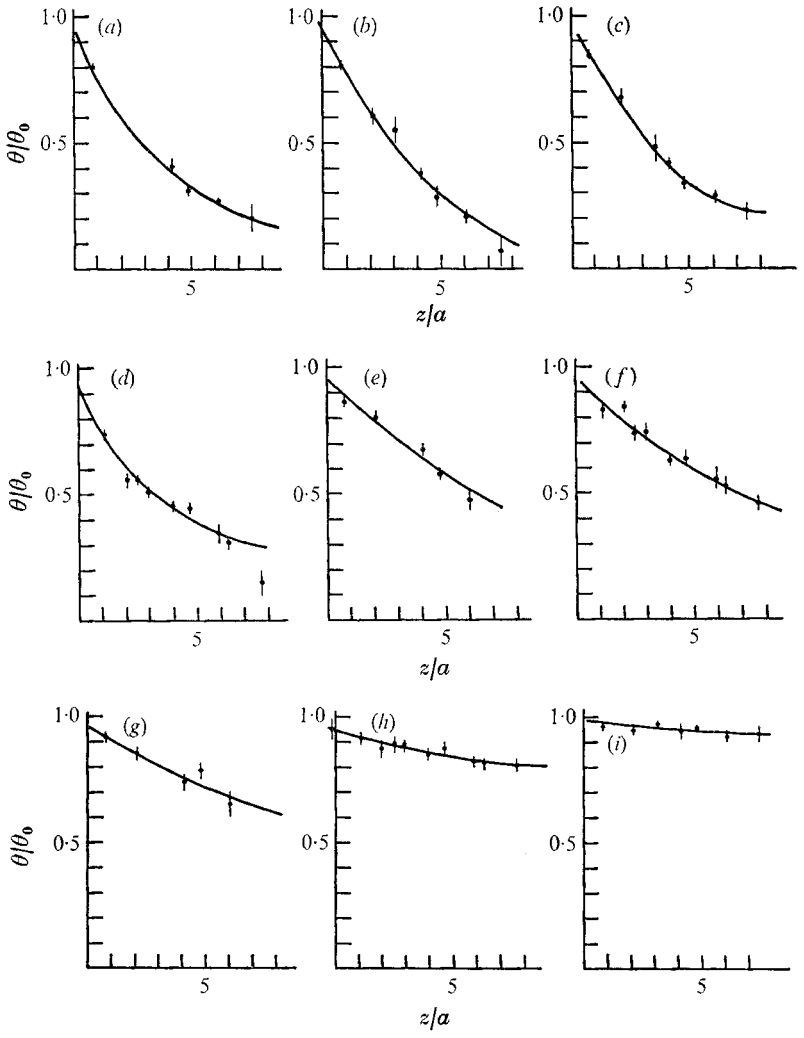

FIGURE 17. Plot of θ/θ_0 against z/a for (*a*) $S = 0{\cdot}24$, (*b*) $S = 0{\cdot}21$, (*c*) $S = 0{\cdot}16$, (*d*) $S = 0{\cdot}14$, (*e*) $S = 0{\cdot}115$, (*f*) $S = 0{\cdot}09$, (*g*) $S = 0{\cdot}08$, (*h*) $S = 0{\cdot}07$, (*i*) $S = 0$.

values in each experiment. The values of the non-dimensional parameters ϵ and E were the same as in the earlier experiments: $\epsilon = 8{\cdot}8 \times 10^{-3}$, $E = 4{\cdot}0 \times 10^{-4}$.

Figures 15 and 16 (plates 3 and 4) show the observed dye profiles at different heights above the obstacle for the cases $S = 0{\cdot}24$ and $S = 0{\cdot}115$ respectively. The differences in magnitude in the distortions as z increases is clearly seen for $S = 0{\cdot}24$. When z/a takes a value of about 7, any distortion of the originally straight dye line becomes difficult to detect. With a lower value of S such as $S = 0{\cdot}115$ the graduations in θ/θ_0 with height, whilst still noticeable, are comparatively less marked. This is illustrated by comparison of figures 15(*d*) and 16(*e*) for $z/a = 6$.

Dye profile observations were taken for each height for several values of S and measurements were made on each to determine the decay rate of θ/θ_0 with

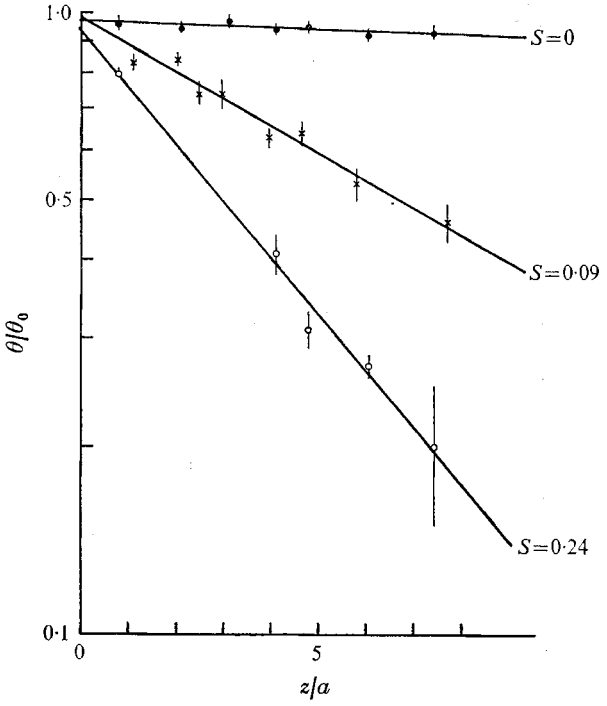

FIGURE 18. Plots of $\log \theta/\theta_0$ against z/a for $S = 0$, $S = 0{\cdot}09$ and $S = 0{\cdot}24$.

z/a, and the dependence of this decay upon S. As mentioned earlier, it was necessary to choose a reference value for θ_0 so that results from different runs could be meaningfully compared. In several cases, for a given (z/a, S) measurement, profiles were obtained where θ_0 differed from the reference value of $\theta_0 = 30°$. In these cases the values of θ/θ_0 were plotted against θ_0 and the measured value of θ/θ_0 for $\theta_0 = 30°$ was obtained.

8.1. *Variation of θ/θ_0 with z/a*

The measured values of θ/θ_0 were plotted against z/a for each S and the graphs are shown in figure 17. Since the decay appeared roughly exponential, $\log \theta/\theta_0$ was plotted against z/a, as shown in figures 18–21. It can be seen that the relationship between $\log \theta/\theta_0$ and z/a is reasonably linear throughout the range of S, within the limits of the experimental error. In particular, with the exception of the graph for $S = 0{\cdot}115$ on figure 21 there does not seem to be a systematic trend in the nonlinearity as S varies. The departure of the $S = 0{\cdot}115$ graph is not thought significant since only five points are plotted and the errors for the lower z/a points are high. The good agreement with an exponential attenuation of θ/θ_0 with height, as illustrated by figures 18–21 enabled an e-folding length to be defined for each S. In order to do this, the best straight lines to the plotted points on figures 18–21 were drawn, and the gradients and intercepts of these lines determined by a least-squares-fit procedure. This procedure incorporated weightings assessed from the standard errors on the points.

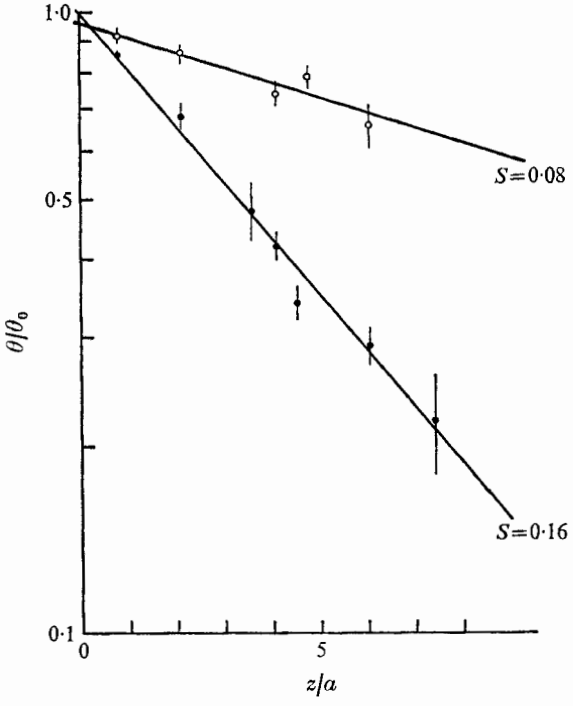

FIGURE 19. Plots of $\log \theta/\theta_0$ against z/a for $S = 0{\cdot}08$ and $S = 0{\cdot}16$.

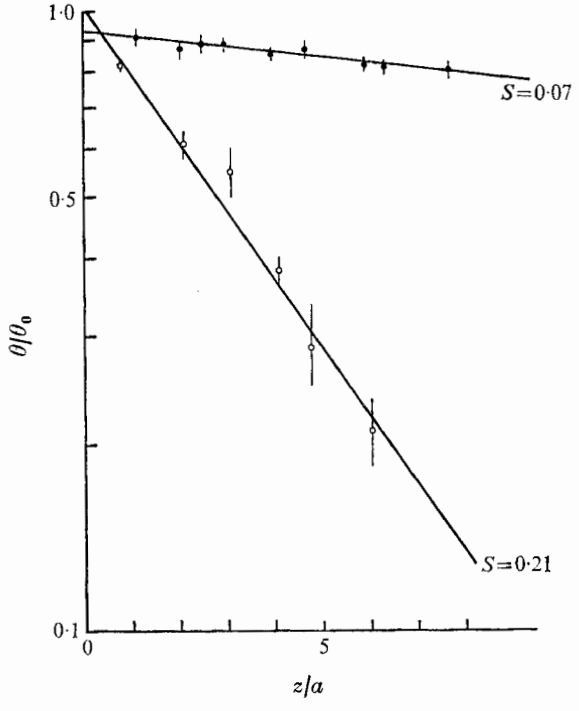

FIGURE 20. Plots of $\log \theta/\theta_0$ against z/a for $S = 0{\cdot}07$ and $S = 0{\cdot}21$.

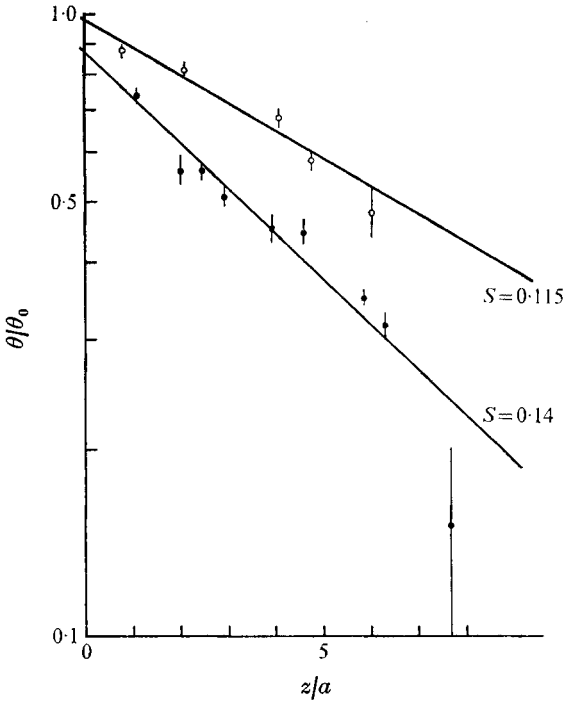

FIGURE 21. Plots of $\log \theta/\theta_0$ against z/a for $S = 0{\cdot}115$ and $S = 0{\cdot}14$.

S	$z_{e/a}$	S	$z_{e/a}$
0	$141{\cdot}0 \pm 21{\cdot}0$	0·14	$6{\cdot}0 \pm 0{\cdot}9$
0·07	$52{\cdot}5 \pm 7{\cdot}8$	0·16	$4{\cdot}8 \pm 0{\cdot}4$
0·08	$18{\cdot}5 \pm 2{\cdot}7$	0·21	$4{\cdot}0 \pm 0{\cdot}5$
0·09	$10{\cdot}2 \pm 1{\cdot}1$	0·24	$4{\cdot}8 \pm 0{\cdot}6$
0·115	$9{\cdot}7 \pm 1{\cdot}0$		

TABLE 1. The length of the Taylor column for various values of S. (Note that for some S, $z_e \gg H$, where H is the height of the fluid region above the top of the sphere. $H/a = 9{\cdot}0$.)

8.2. *Variation of z_e/a with S*

Using the gradients of the best straight-line fits shown on figures 18–21 an e-folding value of z/a, denoted by z_e/a, was calculated for each case. Formally, z_e/a is defined as the normalized height above the top of the obstacle for which the value of θ is $1/e$ times its value θ_0 at the top of the obstacle, for a reference value of $\theta_0 = 30°$. In these experiments z_e/a, the e-folding length, is taken as an arbitrary measure of the length of the Taylor column. The effects of density stratification upon the Taylor column, therefore, are assessed by the effect on z_e/a of varying S. The values of z_e/a calculated from the best least-squares fits to the graphs in figures 18–21 are given in table 1.

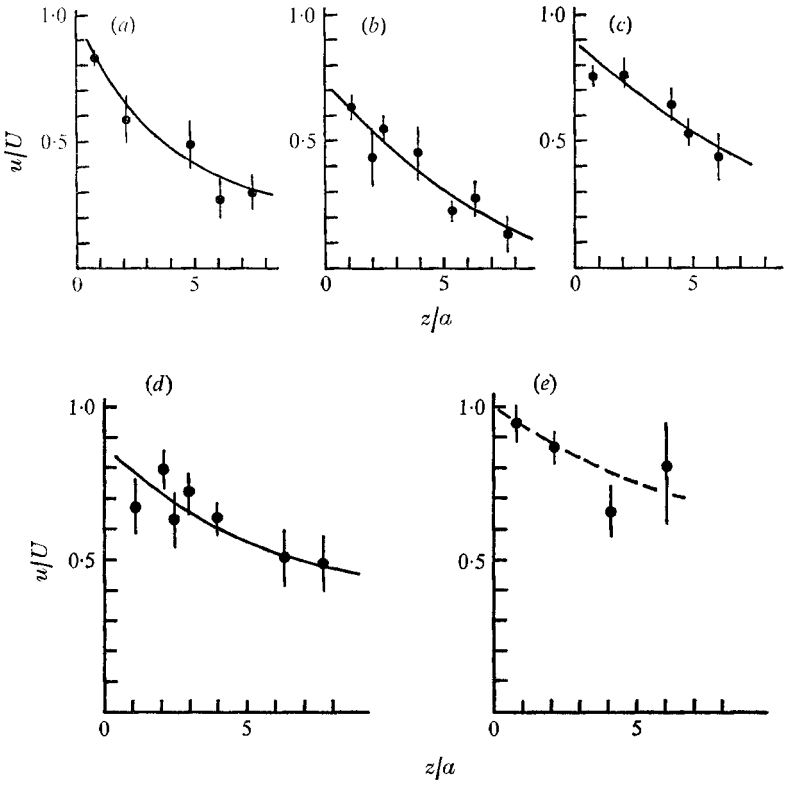

FIGURE 22. Plots of u/U against z/a for (*a*) $S = 0{\cdot}16$, (*b*) $S = 0{\cdot}14$, (*c*) $S = 0{\cdot}115$, (*d*) $S = 0{\cdot}09$, (*e*) $S = 0{\cdot}08$.

8.3. *Velocity measurements*

It was possible in some cases to obtain experimentally some estimates of the mean flow velocities within the column at different heights above the obstacle. Considering a frame of reference fixed in the obstacle, the velocities were measured by recording the motion of the peak of the dye profile for specified time intervals. Because of the experimental configuration, which necessitated a complicated perspective correction procedure, and the short time intervals involved, the velocity measurements were subject to large errors. For a given S and z/a flow velocities could vary considerably within the column with appreciable accelerations and decelerations taking place. In order to make comparisons between interior flow velocities in different experiments, therefore, it was necessary either to compare velocities for certain specified regions of the column or to compare *mean* velocities across the interior. The latter scheme was adopted.

Measurements of these mean velocities u, normalized with the obstacle velocity U, are presented in figure 22 for values of $S = 0{\cdot}16$, $0{\cdot}14$, $0{\cdot}115$, $0{\cdot}09$ and $0{\cdot}08$. A frame of reference fixed in the tank is used so that $u/U = 0$ when no Taylor column is present and u/U takes a value of unity for a 'classical' Taylor column. It is emphasized at this stage that the graphs in figure 22 are plotted from *measured* values of u/U as distinct from the *calculated* velocities appearing in §8.4.

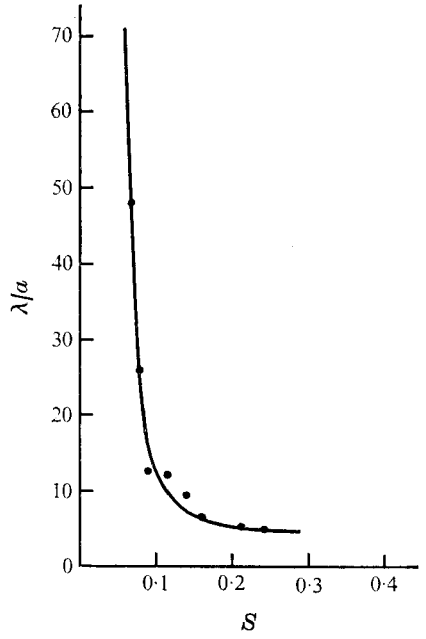

FIGURE 23. Plot of e-folding length λ/a, against stratification parameter S.

The large errors in the points and the scatter of the data make it rather difficult to make any precise estimate of the form of the graphs, but in all cases it can be seen that the gradients of the graphs become steeper as S increases. In this respect these results show good agreement with the results on the vertical motion within the column for zero and non-zero S, as reported in § 5.1.

Direct comparison of the u/U and θ/θ_0 results is not possible, though the relationship between them is simply calculated. Employing the same notation as before, and defining a quantity α such that

$$\alpha = (\theta_0 - \theta) - \beta,$$

where β is the angle subtended by the sphere at O (see figure 14), it can be shown that, for positive α,

$$\alpha/\beta + \theta_0/\theta = U/u(1+\alpha/\beta).$$

Thus, if $\alpha = 0$, i.e. if the dye being observed is still within the column, the quantities θ/θ_0 and u/U are completely equivalent. Alternatively, when the value of θ_0 is chosen such that the peak of any distorted profile is far downstream of the obstacle, α is large and θ/θ_0 is considerably less than u/U.

8.4. *Variation of Taylor-column length with S*

It has been shown in § 8.2 that the e-folding length z_e/a provides a convenient measure of the Taylor-column length. However, though all sets of data presented on figures 18–21 were internally standardized by the choice of a reference value of θ_0, it is clear that the results obtained are dependent upon the specifically chosen θ_0, i.e. $\theta_0 = 30°$. The effect of a change of θ_0 on the trend of these results

is not serious provided that θ_0 is chosen such that $(\theta_0 - \theta) \sim \beta$. However, though the trend is not affected, the 'levelling-off' value of z_e/a at high S is sensitive to changes in θ_0. In order to give the results a general applicability the data were recalculated in terms of velocities using the relationships

$$(U/u)_{\text{calc}} = \begin{cases} 1+\beta/\theta & \text{for} \quad \theta_0 - \theta > \beta, \\ \theta_0/\theta & \text{for} \quad \theta_0 - \theta \leqslant \beta. \end{cases}$$

The above notation is used for the calculated velocities in order to avoid confusion with u/U, the quantity actually measured experimentally, as described in § 8.3. Plots of $(u/U)_{\text{calc}}$ against z, for all the values of S, were made and, as in the graphs of θ/θ_0 against z, an exponential curve through the points was found to be the best fit. Thus, proceeding as before, e-folding lengths were obtained from the $(u/U)_{\text{calc}}$ graphs. Figure 23 shows a plot of λ/a, the e-folding length based on the *calculated* velocity, against S. Each data point (and its associated error) on this figure has been computed from between 30 and 40 experimental measurements.

9. Summary and discussion

Using the method formulated in § 7.1, those modifications to λ, the length of a Taylor column, caused by various degrees of salt-produced density stratification have been investigated. The results are shown on figure 23. This graph shows that λ was severely reduced from its $S = 0$ value by even very slight stratification. For values of less than about 0·15, λ was strongly dependent upon S. For example, a value of $S = 0{\cdot}07$, corresponding to a density difference of 5×10^{-3} gm/cc in a depth of 30 cm, reduced the value of λ by a factor of about three from its 'homogeneous' value. The steep behaviour of the graph is observed up to values of λ of about 0·1, where the length of the column is of the same order as the depth of the tank. As S increases, the reduction in λ becomes more gradual until, after values of S of about 0·15, errors on the graph and approximations in the definition of λ make it difficult to detect any downward trend in the results for increasing S. Between $S = 0{\cdot}15$ and $S = 0{\cdot}25$ the length of the column, as measured by λ, remains essentially constant, having a value of about five sphere radii.

It should be noted that though λ is reduced by a factor of about 30 in the range $0 < S < 0{\cdot}15$, the e-folding length observed at high S is still of the order of half the depth of the tank. In particular, during the experiments no dye profile was observed at any height for any S for which $\theta = 0$.

Hide (1971) has introduced the concept of an axial coherence length to describe the extent to which flow patterns at different heights are steered by bottom topography. From the velocity measurements described in § 8.3 and the measurements of vertical interior motion described in § 5.1 it is possible to make estimates of typical coherence lengths in these experiments. Under the conditions $\sigma \gg 1$, $E \ll 1$ and $\epsilon \ll 1$ it is possible to obtain, from equations (2.6)–(2.8), the thermal wind relationship

$$\rho_0 \left(-2\Omega \frac{\partial v}{\partial z} \right) = g \frac{\partial \rho^*}{\partial x}. \tag{9.1}$$

Considering a co-ordinate system in which u is taken along the local horizontal flow direction and v is thus zero, (9.1) is written, using (2.8), as

$$\rho_0\left(-2\Omega\frac{\partial v}{\partial z}\right) = -g\frac{w}{u}\frac{\partial\overline{\rho}_0}{\partial z}. \tag{9.2}$$

If two levels defined by $z = 0$ and $z = Z$ are situated such that the local direction of horizontal flow at $z = Z$ makes a small angle ψ with the local direction of horizontal flow at $z = 0$, it can be easily shown that

$$\frac{\partial\psi}{\partial z} = \frac{1}{u}\frac{\partial v}{\partial z}. \tag{9.3}$$

Using (9.2) and (9.3), we obtain, after some manipulation,

$$\frac{1}{C} = \frac{\partial\psi}{\partial z} = \frac{1}{a}\frac{w}{u}\frac{U}{u}\frac{S^2}{\epsilon}, \tag{9.4}$$

where C is the Hide coherence length (a, U, S and ϵ are the sphere radius, stream velocity, stratification parameter and Rossby number respectively, as before).

If $w/u \sim \eta/2a$ (see § 5.1) then an order-of-magnitude estimate for C, in terms of quantities measured in the experiments, can be obtained. For the case of $S = 0{\cdot}1$, typical values of $\eta/2a$ and U/u for a height of about $4a$ above the sphere are

$$\eta/a \sim 0{\cdot}2, \quad U/u \sim 1/0{\cdot}75.$$

Thus for $\epsilon \sim 10^{-2}$ an estimated value of C would be $C \sim 5a$. As an order-of-magnitude estimate this is in reasonable agreement with the qualitative results described in § 5, suggesting that, within this range of S, the flow behaviour in certain regions is well represented by the thermal wind equations.

Linear inviscid theory has been applied to the transverse motion of an obstacle through a rotating, stratified, unbounded fluid (Lighthill 1967; Hide 1963; Rao & Rao 1971). In the parameter range of the experiments described here (i.e. $\epsilon^2 \ll 1$, $\epsilon^2 \ll S^2$) it is found that the disturbance produced by the motion of the obstacle has an exponential attenuation in the vertical direction of scale λ^*, where λ^* is given by

$$\left(\frac{\lambda^*}{L}\right)^2 = \left(\frac{1-\epsilon^2}{S^2-\epsilon^2}\right). \tag{9.5}$$

In this expression, L is the horizontal length scale of the obstacle and thus the quantity λ^*/L, by definition, can be thought of as being analogous to the quantity λ/a in figure 23. In the parameter range of the present experiments ($\epsilon^2 \ll 1$, $\epsilon^2 \ll S^2$), therefore, we expect a $1/S$ decay for λ, according to linear inviscid theory. The decay shown by figure 23 is clearly much steeper than $1/S$. However, since the theory of Lighthill (1967) is essentially a far-field theory, which is not expected to describe the behaviour of the fluid near to the forcing region, the discrepancy above is not too surprising in the present experiments.

It was not possible to investigate equation (9.5) very fully: ϵ^2 was always much less than S^2 and hence the effect upon λ of varying ϵ, for constant S, could not be detected. Efforts were made to study the régime where $\epsilon^2 \to S^2$ but in order to keep the Ekman number constant this meant moving the obstacle very quickly or reducing the density gradient. Mixing problems inherent in the latter

and violation of Taylor–Proudman conditions with the former rendered the efforts unsuccessful.

It would appear from the studies of horizontal flow patterns, vertical distortion measurements and velocity measurements that the information obtained is internally consistent, in the sense that even the slightest stratification has been shown to affect strongly all these characteristic features of the flow. This is most clearly seen on figure 23 but is also evident on figure 12, allowing for the scaling differences between the two graphs.

In the case $S = 0$ certain properties of the Taylor column's structure may be inferred from the measurements reported in §§ 4 and 8. The length scale z_c based on measurements of the vertical motion in the column interior, is seen from figure 11 to be of the order $13a$, whilst λ, from figure 23, is about $130a$. That is to say, there is one region in the column in which there exist relatively strong horizontal and vertical motions, and another region in which the flow is affected by the presence of the obstacle though essentially no vertical motion is observed. The measurements mentioned earlier indicate that the vertical extent of these two regions differs by an order of magnitude. In view of this difference, therefore, it becomes very important when referring to Taylor columns in laboratory or geophysical situations, to specify precisely which particular Taylor-column definition is being used. This problem of definition, briefly indicated in the introductory remarks of § 7.1, has recently been discussed by Hide (1971).

Following the definition adopted in the present experiments and regarding λ as the Taylor-column length, it is of interest to note that the value obtained in the $S = 0$ case is of the same order as the theoretical estimate $(1/\epsilon)$ of Lighthill (1967) for the Rossby number ($\epsilon = 8{\cdot}8 \times 10^{-3}$) in these experiments. This theoretical estimate, though based on an inviscid model in which the column's extent is limited by inertial effects only, does nevertheless provide an upper limit for comparison with the present experiments. The importance of the role played by viscous forces can be gauged from the theoretical condition obtained by Jacobs (1964*a*); i.e. inertial effects can be neglected if ϵ and E satisfy the inequality $\epsilon \ll E^{\frac{1}{2}}$. From § 8 it is seen that the quantities ϵ and $E^{\frac{1}{2}}$ are of the same order in these experiments. In view of the good agreement between λ and $1/\epsilon$ (Lighthill 1967), this therefore suggests that viscous effects have not strongly affected the Taylor-column length in the $S = 0$ case.

This work, based on part of the author's Ph.D. research, was carried out in the School of Physics, The University of Newcastle upon Tyne. The help and interest of, particularly, Dr D. J. Tritton, who supervized the work and contributed helpful criticisms of the manuscript, is gratefully acknowledged. Dr C. W. Titman, who designed the rotating table, and Dr A. Ibbetson, are thanked for their considerable help, and the Science Research Council for their financial support. The work has been completed at the International Meteorological Institute in Stockholm, during the tenure of a post-doctoral fellowship award from the Royal Society. Thanks are due to Gösta Walin of the above institute for his comments on the manuscript, and to Miss Inger Albrecktsson for help with the drawings.

REFERENCES

BAKER, D. J. 1966 A technique for the precise measurement of small fluid velocities. *J. Fluid Mech.* **26**, 573.

DAVIES, P. A. 1971 Experiments on Taylor columns in rotating stratified fluids. Ph.D. thesis, University of Newcastle upon Tyne.

HIDE, R. 1961 Origin of Jupiter's Great Red Spot. *Nature*, **190**, 895.

HIDE, R. 1963 On the hydrodynamics of Jupiter's atmosphere. *Mem. Soc. Roy. Sci. Liege, Ser* V, **7**, 481.

HIDE, R. 1969 Dynamics of the atmospheres of the major planets, with an appendix on the viscous boundary layer at the rigid bounding surface of an electrically-conducting rotating fluid in the presence of a magnetic field. *J. Atmos. Sci.* **26**, 841.

HIDE, R. 1971 On geostrophic motion of a non-homogeneous fluid. *J. Fluid Mech.* **49**, 745.

HIDE, R. & IBBETSON, A. 1966 An experimental study of 'Taylor columns'. *Icarus*, **5**, 279.

HIDE, R., IBBETSON, A. & LIGHTHILL, M. J. 1968 On slow transverse flow past obstacles in a rapidly rotating fluid. *J. Fluid Mech.* **32**, 251.

IBBETSON, A. 1965 Ph.D. thesis, University of Durham.

JACOBS, S. J. 1964*a* The Taylor column problem. *J. Fluid Mech.* **20**, 581.

JACOBS, S. J. 1964*b* On stratified flow over bottom topography. *J. Mar. Res.* **22**, 223.

LIGHTHILL, M. J. 1967 On waves generated in dispersive systems by travelling forcing effects, with applications to the dynamics of rotating fluids. *J. Fluid Mech.* **27**, 725.

OSTER, G. 1965 Density gradients. *Scientific American*, no. 70.

PROUDMAN, J. 1916 On the motion of solids in a liquid possessing vorticity. *Proc. Roy. Soc.* A **92**, 408.

RAO, V. S. & RAO, G. V. P. 1971 On waves generated in rotating stratified liquids by travelling forcing effects. *J. Fluid Mech.* **46**, 447.

ROBINSON, A. R. 1960 On two-dimensional intertial flow in a rotating stratified fluid. *J. Fluid Mech.* **9**, 321.

STEWARTSON, K. 1953 On the slow motion of an ellipsoid in a rotating fluid. *Quart. J. Mech. Appl. Math.* **6**, 141.

STEWARTSON, K. 1967 On slow transverse motion of a sphere through a rotating fluid. *J. Fluid Mech.* **30**, 357.

STONE, P. H. & BAKER, D. J. 1968 Concerning the existence of Taylor columns in atmospheres. *Quart. J. Roy. Met. Soc.* **94**, 576.

TAYLOR, G. I. 1923 Experiments on the motion of solid bodies in rotating fluids. *Proc. Roy. Soc.* A **104**, 213.

VAZIRI, A. & BOYER, D. L. 1971 Rotating flow over shallow topographies. *J. Fluid Mech.* **50**, 79.

WARREN, B. A. 1963 Topographic influences on the path of the Gulf Stream. *Tellus*, **15**, 167.

WARREN, B. A. 1969 Divergence of isobaths as a cause of current branching. *Deep Sea Res.* **16**, 339 (Fuglister Anniversary Volume).